Changes in extreme regional sea level under global warming

S.-E. Brunnabend[1,2], H. A. Dijkstra[1], M. A. Kliphuis[1], H. E. Bal[3], F. Seinstra[4], B. van Werkhoven[4], J. Maassen[4], and M. van Meersbergen[4]

[1]Institute of Marine and Atmospheric Research Utrecht, Utrecht University, Princetonplein 5, 3584 CC Utrecht, The Netherlands.
[2]Institute for Geodesy and Geoinformation, Bonn University, Bonn, Germany.
[3]Department of Computer Science, VU University Amsterdam, 1081 HV Amsterdam, The Netherlands.
[4]Netherlands eScience Center, 1098 XG Amsterdam, The Netherlands.

Correspondence to: Sandra-Esther Brunnabend (brunnabend@geod.uni-bonn.de)

Abstract. An important contribution to future changes in regional sea level extremes is due to the changes in intrinsic ocean variability, in particular ocean eddies. Here, we study a scenario of future dynamic sea level (DSL) extremes using a strongly eddying version of the Parallel Ocean Program. This model is forced with atmospheric fluxes from a coupled climate model which has been inte-

5   grated under the IPCC-SRES-A1B scenario over the period 2000-2100. Changes in 10-year return time DSL extremes are very inhomogeneous over the globe and are related to changes in ocean currents and corresponding regional shifts in ocean eddy pathways. In this scenario, several regions in the North Atlantic experience an increase in mean DSL of up to 0.4 m over the period 2000-2100. DSL extremes with a 10-year return time increase up to 0.2 m with largest values in the northern and

10 eastern Atlantic.

1 Introduction

From satellite measurements, it has been well established that global mean sea level has increased by about 3 mm/yr over the period 1993-2010 (Rhein et al., 2013; Church and White, 2011; Church et al., 2013; Watson et al., 2015). However, regional sea level trends are very inhomogeneous over

15 the oceans, and range from about a 10 mm/yr increase in the western tropical Pacific to about 5 mm/yr decrease in the subtropical eastern Pacific (Church et al., 2013). Regional deviations from global mean sea level occur due to ocean warming, global isostatic adjustment, land-ice mass loss and changes in the ocean circulation. The dynamic sea level (DSL) component is the sum of the contributions from local steric (thermal and saline) effects and ocean mass redistribution.

20   Until 2100, global mean sea level is projected to rise up to roughly one meter depending on the climate change scenario considered (Slangen et al., 2012, 2014). For example, under the SRES-A1B scenario, the global mean sea level is likely to rise between 0.42 m and 0.8 m (compared to

1986-2005), with major contributions provided by thermal expansion of ocean water and the mass loss of the major ice sheets and glaciers (Church et al., 2013; Slangen et al., 2014). For the highest radiative forcing scenario (RCP8.5), projected global sea level rise is between 0.52 and 0.98 m in 2100 (Church et al., 2013). Regional sea level changes projected for the North Atlantic show complex patterns that are partly caused by a weakening of the Atlantic Meridional Overturning Circulation (AMOC), by a shift in the path of the North Atlantic Current, and by changes in surface buoyancy fluxes (Landerer et al., 2007; Yin et al., 2010, 2009; Pardaens et al., 2011; Kienert and Rahmstorf, 2012; Bouttes et al., 2013). Thermosteric sea level evolves with a pattern that reflects the reduced heat transport to the North Atlantic due to changes in ocean currents (Yin et al., 2010; Pardaens et al., 2011). For example, DSL is rising near the North American continent because of a reduction in the AMOC causing a redistribution of ocean mass (Landerer et al., 2007; Yin et al., 2009, 2010; Bouttes et al., 2013).

The spread in the projections of regional sea level change is largely determined by internal ocean variability and model uncertainty. In Slangen et al. (2012) and Bordbar et al. (2015), the spread due to decadal-to-centennial variability is considered by looking at ensemble simulations using CMIP3 and CMIP5 climate models, respectively. It was shown that the (CMIP5) ensemble spread of the projected DSL is of the same order of magnitude as the globally averaged sea level rise (Bordbar et al., 2015). Several regions were identified where the forced sea level change signal is relatively strong with respect to the internal variability, e.g. the Indo-Pacific part of the Southern Ocean and the eastern equatorial Pacific and hence may be detected earlier (Bordbar et al., 2015).

However, in all these model studies the strongest component of oceanic internal variability, i.e. that due to ocean meso-scale eddies, was not represented. Rectification processes due to eddies can lead to strong changes in mean ocean surface flows and their response to atmospheric forcing, in particular in the Southern Ocean (Böning et al., 2008). In strongly eddying ocean models even new modes of low-frequency variability may appear, such as the multidecadal Southern Ocean Mode (Bars et al., 2016). Using the eddy-permitting (about $1/4°$ horizontal resolution) version of the MIROC3.2 model, Suzuki et al. (2005) showed that representing ocean eddies provides a more detailed projection of regional sea level changes under the IPCC SRES-A1B scenario and that eddies are strongly involved in regional sea level extremes. In addition, as demonstrated by Firing and Merrifield (2004) from observational data, a high background sea level superposed on the sea level change due to an arriving ocean eddy can lead to extreme local sea levels.

Eddies can also have a strong effect on the deep ocean circulation, in particular the AMOC. The study of Weijer et al. (2012) indicates that the AMOC in the strongly eddying (about $0.1°$ horizontal resolution) version of the POP model version is more sensitive to freshwater perturbations than the non-eddying version of the same model. Climate model studies on the projections of the AMOC with non-eddying ocean components show only an AMOC decline of 22% to 40% over the period 2000-2100, depending on the IPCC scenario (Weaver et al., 2013). Only two (out of 30) of these

60   models project a substantial decrease of the AMOC under the RCP8.5 scenario. However, in high-resolution ocean models strong variations in the AMOC strength lead to changes in ocean currents and eddy pathways, which induce an additional contribution to the variability in DSL and hence affect extreme DSL values (Brunnabend et al., 2014).

   It is important to assess the role of eddies in projections of future regional sea level changes, in

65   particular on the DSL extremes. In this paper, we study a scenario of future DSL change using the strongly eddying version of POP as in Brunnabend et al. (2014), but now forced with atmospheric fields from a coupled climate model that evolved under the SRES-A1B scenario. We focus on the changes in the probability density function of regional (and more local) DSL values and 10-year return extreme values over the period 2000-2100 and compare these results to those obtained from a

70   similarly forced non-eddying version of POP.

2   Ocean model

The high-resolution version of the POP used has a spatial resolution of 0.1° horizontally and 42 depth levels of which the thickness varies from 10 m near the surface to 250 m near the ocean bottom (Maltrud et al., 2008). The high spatial resolution captures the processes leading to meso-

75   scale ocean eddies and provides a more detailed representation of the western boundary currents. Specific details about the high-resolution model setup, such the treatment of the bottom topography, sea ice and river runoff, are described in the Weijer et al. (2012). The high-resolution model was optimised for use on the Cartesius supercomputer in Amsterdam (www.surfsara.nl) and about 3 model years are simulated per 24h using about 1000 cores.

80   The POP simulation was initialised from a 75 year spin-up simulation (Maltrud et al., 2008) under the CORE-I climatology dataset (Large and Yeager, 2004) as atmospheric forcing. This initial condition is indicated here as the year 1950. Under a freshwater flux which is diagnosed from the last five years of this spin-up, the model displays only a very small drift over a 200 year control simulation (Bars et al., 2016). Here, the model was forced with monthly mean atmospheric forcing fluxes over

85   the period 1950-2100, that were derived from simulations with the ECHAM5-OM1 model within the ESSENCE (Sterl et al., 2008) project (see www.knmi.nl/~sterl/Essence/). The used forcing fields are 10 m wind speed, downward flux of short wave and longwave radiation, 2 m temperature, humidity, precipitation, runoff, and the surface wind stress field. The atmospheric forcing fields are given on a global 1° × 1° grid and are interpolated to the curvilinear POP model grid. The outgoing heat and

90   freshwater fluxes are computed within the model using bulk formulae. There is an initial adjustment after the switch in forcing in 1950, for example measured by the change in the AMOC strength, which lasts for about a decade.

   Over the years 1950-2000, the POP model was forced by the ensemble mean atmospheric fields from the ESSENCE project that take observed concentrations of greenhouse gases and anthro-

95   pogenic aerosols into account. Over the years 2001-2100, POP was forced with atmospheric forcing
     fields obtained from the ECHAM5-OM1 model according to the SRES A1B scenario (from an ar-
     bitrarily chosen ensemble member of the ESSENCE project (Sterl et al., 2008)). We choose ensem-
     ble member #021 for which the high-resolution simulation is denoted by R_{021}. In addition to this
     high-resolution simulation, a similarly forced simulation is performed with the low resolution POP

100 version, indicated in the following by R_{021}^{low}. This non-eddying version has an average 1.0° horizontal
     resolution and 40 vertical levels (Weijer et al., 2012). The Gent and McWilliams (1990) scheme is
     used to represent eddy-driven tracer transports. Such a scheme is not needed in the strongly eddying
     version as these tracer transports are explicitly resolved.

     The POP model directly computes the DSL, which can be decomposed into a mass redistribution

105 term and a steric contribution. Because the freshwater flux is included into the model as a virtual
     salt flux and the global mean of precipitation, evaporation and river runoff is zero, no mass induced
     global mean sea level changes can be represented. Due to the applied Boussinesq approximation,
     global mean steric sea level variations are not accounted explicitly during this study but this spatially
     independent contribution was computed from the model output (Greatbatch, 1994).

110 To demonstrate the performance of both versions of the POP model, we compare the DSL over the
     years 1993-2012 (computed from monthly means) with observations derived from altimetry. White
     areas indicate the sea-ice regions where restoring conditions are applied in POP and hence these
     are not considered in the analyses below. The mean DSL of simulation R_{021} over years 1993-2012
     agrees well with observations, both for the mean (compare Fig. 1a and Fig. 1c) and the standard

115 deviation (compare Fig. 1b and Fig. 1d). This shows that the model adequately determines the mean
     ocean circulation, including the western boundary currents and also represents the eddy-induced
     variability. Differences with respect to observations appear due to the general overestimation of the
     modeled variability during this time period, which may be due to the prescribed low resolution of the
     atmospheric forcing and the lack of feedback of the atmosphere on the ocean variability. Differences

120 in variability may also occur due to the higher horizontal resolution of the ocean model (0.1°) than
     the altimetry dataset used (0.25°) as more small-scale features can be resolved. Regional differences
     in variability in the South Atlantic are caused by a too regular Agulhas ring formation rate in POP
     compared to observations (Bars et al., 2014).

     In contrast, results for the low resolution simulation R_{021}^{low} shown in Fig. 1e (mean) and Fig. 1f

125 (standard deviation) indicate that only the mean DSL change is reasonable well captured. The model
     shows too low variability, in particular in the regions of the western boundary currents similar to
     many other non-eddying ocean model results (Bordbar et al., 2015). This weak variability also has
     consequences for the mean flow through the lack of representation of rectification processes causing,
     for example, too small DSL values in the Agulhas and the Gulf Stream regions.

130 ## 3   Future dynamic sea level changes

In the results below, all long term changes are computed by taking the difference between values over the last 20 years (2081-2100) and the first 20 years (2001-2020) of the model simulations. Monthly mean data are used for the analysis of changes in the mean and standard deviation (section 3.1), while daily data are used in the extreme value analyses (section 3.2).

135 ### 3.1   Mean and standard deviation

In the POP simulation R_{021}, global mean steric height increases by about 2.2mm/yr from year 2000 to 2100. As this signal is homogeneous over the Earth, it is not considered in the results below. Largest changes in mean DSL between the periods 2081-2100 and 2001-2020 occur in the North Atlantic (Fig. 2a), in particular near the western part of this basin (Fig. 2c). There is a mean DSL

140 decrease in the Atlantic and Pacific parts of the Southern Ocean, while mean DSL increases in the Indian part of the Southern Ocean. The mean DSL increases in the eastern part of the North Atlantic basin and decreases in the center of the subpolar gyre. Large changes in DSL variability occur in the Agulhas retroflection region and near Drake Passage (Fig. 2b). The DSL variability decreases in the western North Atlantic, in the center of the subpolar gyre and slightly along the western boundary

145 of the North Atlantic while it substantially increases in the eastern Atlantic (Fig. 2d).

In the POP simulation R_{021}^{low}, global mean steric height varies only by a few cm over the period 2000 to 2100 and again is not considered further. Regarding mean DSL patterns and amplitudes, the results of the low resolution simulation (R_{021}^{low}), as shown in Fig. 2e, agree well with many other model studies using non-eddying ocean models (Landerer et al., 2007; Yin et al., 2009, 2010; Bord-

150 bar et al., 2015). At first sight, the results also look similar to those for the R_{021} simulation (compare Fig. 2a and Fig. 2e). However, when regional details are considered, the results are different. The Southern Ocean basin contrast (Indian versus Atlantic/Pacific) is much stronger in the R_{021} results. The DSL change in the Northern Atlantic is more dipolar in the North Atlantic in the R_{021}^{low} results, with a large area south of Greenland with decreasing mean DSL. The change in DSL variability is, as

155 expected, different in both models (compare Fig. 2b and Fig. 2f), in particular in western boundary current regions. In the North Atlantic, (compare Fig. 2d and Fig. 2h), the changes in variability are less coherent in the Gulf Stream region and have larger amplitudes in the eastern part of the basin.

To explain the changes in DSL in the North Atlantic (Fig. 2c-d), the behavior of the Atlantic Meridional Overturning Circulation (AMOC) is shown in Fig. 3. The maximum AMOC at 26°N

160 decreases from about 20 Sv to about 5 Sv (red curve in Fig. 3a). The spatial pattern of the AMOC is not changing but the North Atlantic Deep Water is shallowing by about 1000 m (Fig. 3b-c). The maximum strength of the AMOC at 35°S decreases (blue curve in Fig. 3a) by more 60%. The decline in the AMOC causes a rise in mean DSL of up to 0.4 m near the North American continent, mostly because of a redistribution of ocean mass towards these regions (cf. Fig. 1a). The reduction of the

165   AMOC in the R_{021}^{low} simulation (not shown) is only a few Sv, as in the ESSENCE ensemble (Sterl et al., 2008; Van Oldenborgh et al., 2009).

     The reduction of the AMOC also causes a northward shift of the latitude separation of the Gulf Stream. This result has also been found in the non-eddying model studies (Landerer et al., 2007) and previous strongly eddying model studies (Brunnabend et al., 2014). In addition, eastward shifts

170   of the path of the Gulf Stream and North Atlantic Current occur. This is shown more clearly by the change in surface mean kinetic energy (Fig. 4a) which has decreased over most of the Gulf Stream path in the R_{021} simulation. Fig. 4c and 4d show the change of the eddy kinetic energy (EKE) of year 2090 with respect to 2010. The changes in the mean current path redirect eddies and lead to higher variability in the eastern Atlantic while in the sub-polar region the variability is reduced. In the

175   R_{021}^{low} simulation, similar shifts in the current system in the North Atlantic occur (Fig. 4b). However, the amplitude of the kinetic energy changes is much smaller compared to the R_{021} simulation, in particular in the Labrador Sea and in the Caribbean Sea.

     In the R_{021} simulation, the global mean sea surface temperature (SST) rises by about 2°C over the period 2000-2100 (Fig. 5a). Almost all ocean regions experience a warming and near the east

180   coast of North America, there is a warming of up to 4°C. However, in the subpolar gyre region of the North Atlantic, SST is decreasing by more than 3°C. SST remains almost unchanged over large regions in the Southern Ocean. This can be explained by the atmospheric forcing fields associated with the SRES-A1B scenario as they lead to changes in the radiative forcing between atmosphere and ocean. In addition, the decrease of the AMOC strength reduces the heat transport to the northern

185   polar regions, which cools the upper ocean in the subpolar region. This leads to thermal contraction, and a negative DSL change(Fig. 2a).

     The DSL change in the Southern Ocean between the periods 2081-2100 and 2001-2020 (Fig. 2a) is caused by a southward shift of the westerly winds. In addition, the westerly wind stress strengthens by about 0.03 Pa (Fig. 5b). The increase in zonal momentum flux accelerates the Antarctic Circum-

190   polar Current and increases the northward Ekman transport that changes the slope of the isopycnal surfaces in the South Atlantic (Yin et al., 2010). These effects cause changes in the water mass properties leading to steric contraction in the Southern Ocean and steric expansion in the region of the Agulhas return current (Yin et al., 2010), explaining the results in Fig. 2a.

     The reduction of the AMOC also decreases the ocean-atmosphere temperature difference in the

195   subpolar Atlantic region and hence leads to a reduction in the net ocean-atmosphere surface heat flux, i.e. a reduced heat loss to the atmosphere (Fig. 5c). The cooling leads to reduced evaporation resulting in a freshening of the upper ocean (Fig. 5d), which causes a further slowdown of the AMOC as the AMOC is particularly sensitive to freshwater anomalies in this region (Smith and Gregory, 2009; Weijer et al., 2012). The changes in surface fluxes for the simulation R_{021}^{low} (not shown) are very

200   similar as they are derived from the same atmospheric forcing fields, and are only slightly differently affected by the ocean fields, compared to the R_{021} simulation. Because the mechanism of deep water

formation is very different in the low-resolution model, the AMOC responds more mildly to changes
in surface forcing than that in the high-resolution model (Weijer et al., 2012).

3.2 Regional PDF and Extremes

205 To determine an estimate of the Probability Density Function (PDF) of DSL we show histograms of
modelled daily-mean DSL data over two 20 year periods (2001-2020 and 2081-2100). To remove
variations on long time scales, all signals with frequencies lower than 550 days are first filtered out of
these DSL time series. This leaves the seasonal and annual signals in the DSL time series and hence
changes on these time scales also lead to changes in the PDFs and the DSL extremes. The PDFs are

210 computed for three different regions in the North Atlantic (as shown in Fig. 6) using the daily-mean
maximum value (over the region) in each of the regions from the daily-mean time series. The PDFs
for three specific locations near the Azores, the Bermuda Islands, and Lisbon are also computed by
using the monthly maximum value (at that location) from the daily time series.

The changes in each PDF for the R_{021} simulation for the different regions and locations are

215 plotted in Fig. 7 with the blue histogram being the future PDF. The variance of DSL decreases in
mid-Atlantic region 1 (cf. Fig. 2b,d), which is seen by the shift of the PDF to the left (Fig. 7a). This
also leads to a reduction of the highest DSL extremes by more than 10 cm. In region 2 (western North
Atlantic) DSL is mainly driven by mean changes due to steric effects and the mass redistribution and
hence the PDF shifts to the right (Fig. 7b). In the eastern North Atlantic (region 3), the variance of

220 the DSL increases (cf. Fig. 2b,d) due to the changes in the pathways of eddies causing the changes
in EKE (Fig. 4c,d). This leads to a rightward shift of the PDF by about 10 cm in this region (Fig.
7c).

Changes in the pathways of eddies are also important when considering local DSL extremes. The
Azores are located in a region of slightly decreased variability (Fig. 1b,d) due to reduced eddy-

225 kinetic energy in this region, shifting the PDF slightly to the left (Fig. 7d). Near the Bermuda Islands
the shift in the ocean currents leads to lower probabilities of higher sea level extremes. (Fig. 7e).
The most interesting result, however, is shown in Fig. 7f for the coast near Lisbon. Due to the shift
in the Gulf Stream and North Atlantic Current one would expect increased probabilities for high
DSL values in this region. However, because these currents are not only shifted but also reduced in

230 strength almost no changes in DSL extremes can be identified (Fig. 7f).

The changes in the PDFs for the R_{021}^{low} simulation show quite a different behavior than those in the
R_{021} simulation for most regions and locations. While the relative shift in the mean is comparable
for both models in the regions 1 and 2 (Fig. 8a,b), the amplitude is much smaller for R_{021}^{low}. For
region 3 (Fig. 8c), the PDF has bimodal characteristics and hardly changes under climate change,

235 in contrast to the change in the R_{021} simulation (Fig. 7c). The PDF change for the Azores is the
opposite (Fig. 8d) in both models due to the fact that the eastward shift in the Gulf Stream has no

influence on ocean eddy paths in the R_{021}^{low} simulation (Fig. 4b). The PDF of the other two locations (Fig. 8e,f) show the same behavior as in the R_{021} simulation.

The extreme DSL values for a specific return time are computed here in the same way as in
240   Brunnabend et al. (2014). i.e. from a fit of parameters in a Generalized Extreme Value (GEV) distribution (Coles, 2001). The extreme DSL values at a return time of 120 months (10 years) over the period 2001-2020 and their changes over the different 20 year periods (2081-2100 and 2001-2020) of the R_{021} simulation are shown in Fig. 9. Over the period 2000-2020 higher extreme sea levels occur in regions of high variability, i.e. in regions of the major current systems such as the Gulf Stream
245   and the Agulhas Current (Fig. 9a,c). Therefore, the regional pattern of changes in extreme sea levels for a return time of 10 years (Fig. 9b,d) reflects the changes in sea level variability as shown in Fig. 2b,d. Sea level extremes can increase by 50 cm near Tasmania. Furthermore, in the northern and eastern North Atlantic, sea level extremes with a 10-year return time will increase by up to 20 cm. A comparison of the PDFs and the DSL extremes (for the 10 year return time) using a 550-day filter
250   and a 180-day filter (not shown) indicates that the change in DSL extremes are dominated by the change in short term variability caused mainly by the shift in the ocean currents changing the eddy pathways (Fig. 4c-d).

The same extreme sea level values are shown in Fig. 10 for the R_{021}^{low} simulation. The amplitude of these extremes is much smaller, in particular in western boundary current regions (Fig. 10a) and
255   in the Gulf Stream region (Fig. 10c). The low-resolution ocean model simulation leads to different extreme sea level projections in the northern North Atlantic (in particular, in the Labrador Sea and Barents Sea) than for the R_{021} simulation. The sign of the change in sea level extremes is also different in the Caribbean Sea. This shows the importance of including an explicit representation of eddy processes into an ocean model when looking at regional projections of DSL.

260   **4   Summary and Discussion**

In this paper, we considered a single realisation of future dynamic sea level (DSL) changes using a strongly eddying ocean model forced by atmospheric fields according to an SRES A1B scenario. The results show that changes in local and regional PDFs (between the periods 2001-2020 and 2081-2100) are mainly due to changes in DSL variability on short time scales and therefore related to
265   changes in the ocean eddy field. This can be deduced from both the changes in the eddy kinetic energy of the ocean surface velocity field and from a comparison of DSL changes in a non-eddying version of the same model. In the high-resolution model simulation, the changes in eddy pathways are caused by a strong decrease of the AMOC with simultaneous eastward shifts in the path of the Gulf Stream and North Atlantic Current.

270   Our main result is that the pattern of 10-year return time DSL extremes (as shown in Fig. 9) are determined by changes in the ocean eddy field (Suzuki et al., 2005; Brunnabend et al., 2014). In

some regions of the globe these extreme DSL values can be up to 0.5 m which of the same order of magnitude as the mean DSL change. This shows the importance of internal ocean variability for regional extreme sea levels, not only on the longer time scales (Bordbar et al., 2015), but also on the shorter time scales (Firing and Merrifield, 2004).

Low resolution ocean/climate models are not capable of accurately representing these changes in extreme sea levels. Some low resolution model studies do capture a shift in ocean currents in case of a declining AMOC (Landerer et al., 2007; Yin et al., 2010, 2009; Pardaens et al., 2011; Kienert and Rahmstorf, 2012). However, the model resolution is not resolving DSL variability caused by ocean eddies, as the parameterisation of eddies in these models only affects the heat and salt transport in the models. Already using an eddy-permitting ocean/climate model (with a 0.25° horizontal resolution) indicated the importance of resolving ocean eddies to accurately estimate future sea level variability (Suzuki et al., 2005), but in these models the western boundary currents usually do not have a correct separation behaviour.

There are several caveats in this model study which may modify the results quantitatively but which do not affect the main message of this paper that strongly eddying models are important for regional future sea level change projections. First, the AMOC in the R_{021} POP model simulation appears to be very sensitive to freshwater anomalies and hence the scenario here may be quite an extreme one. Second, the usage of an ocean-only model with mixed boundary conditions below sea-ice regions and atmospheric forcing fields from a climate model is restricting the capabilities of the model in simulating the coupled ocean-atmosphere interactions occurring in reality. However, it is expected that shifts in the ocean eddy fields would also occur in coupled models with strongly eddying ocean model components. Third, the model does not simulate many other processes causing regional and coastal sea levels changes (e.g. GIA, and gravity). Many of these processes would only effect the mean DSL values and not its variability. Hence, as a first approximation, these sea level changes can be added to the mean DSL values (Slangen et al., 2012, 2014) determined here. Finally, we studied only one realization of the model here and it would be better to use an ensemble of simulations (Bordbar et al., 2015) to determine the effect of ocean initial conditions and to have better statistics on the extreme DSL values. The latter is still hardly feasible with the current computational capabilities.

We conclude from the results that when developing plans for adapting to future changing sea level, not only mean regional changes should be considered, although they may be substantial. Also the changes in variability should be accounted for, as with higher variability the probability of sea level extremes may increase. This in particular holds for the North Atlantic region where many areas are vulnerable to sea level rise.

Acknowledgements. This study was supported by the Netherlands eScience Center (NLeSC) through the eSALSA (An eScience Approach to determine future Sea-level chAnges) project. The simulations have

been performed on the Cartesius supercomputer at SURFsara (https://www.surfsara.nl) through the project
SH-243-13. This work was also partially funded by the Dutch national research program COMMIT. The

310   altimeter products were produced by Ssalto/Duacs and distributed by Aviso, with support from Cnes
(http://www.aviso.altimetry.fr/duacs/). To get access to the POP model results please write an email to the
corresponding author.

References

Bars, D. L., Durgadoo, J. V., Dijkstra, H. A., Biastoch, A., and Ruijter, W. P. M. D.: An observed 20-year time series of Agulhas leakage, Ocean Science, 10, 601–609, doi:10.5194/os-10-601-2014, 2014.

Bars, D. L., Viebahn, J. P., and Dijkstra, H. A.: A Southern Ocean mode of multidecadal variability, Geophysical Research Letters, 43 (5), 2102–2110, 10.1002/2016GL068177, 2016.

Böning, C. W., Dispert, A., Visbeck, M., Rintoul, S. R., and Schwarzkopf, F. U.: The response of the Antarctic Circumpolar Current to recent climate change, Nature Geoscience, 1, 864 – 869, doi:10.1038/ngeo362, 2008.

Bordbar, M. H., Martin, T., Latif, M., and Park, W.: Effects of long-term variability on projections of twenty-first-century dynamic sea level, Nature Climate Change, 5, 343–347, doi: 10.1038/NCLIMATE2569, 2015.

Bouttes, N., Gregory, J. M., Kuhlbrodt, T., and Smith, R. S.: The drivers of projected North Atlantic sea level change, Climate Dynamics, 43, 5, 1531–1544, doi: 10.1007/s00382-013-1973-8, 2013.

Brunnabend, S.-E., Dijkstra, H. A., Kliphuis, M. A., van Werkhoven, B., Bal, H. E., Seinstra, F., Maassen, J., and van Meersbergen, M.: Changes in extreme regional sea surface height due to an abrupt weakening of the Atlantic meridional overturning circulation, Ocean Science, 10, 881–891, doi: 10.5194/os-10-881-2014, 2014.

Church, J. A. and White, N. J.: Sea-Level Rise from the Late 19th to the Early 21st Century, Surveys in Geophysics, 32, 585–602, doi: 10.1007/s10712-011-9119-1, 2011.

Church, J. A., Clark, P. U., Cazenave, A., Gregory, J. M., Jevrejeva, S., Levermann, A., Merrifield, M. A., Milne, G. A., Nerem, R. S., Nunn, P. D., Payne, A. J., Pfeffer, W. T., Stammer, D., and Unnikrishnan, A. S.: Sea Level Change, in: The Scientific Basis, Contribution of Working Group I to the Fifth Assessment Report of the Intergovernmental Panel on Climate Change, edited by Stocker, T. F., Qin, D., Plattner, G.-K., Tignor, M., Allen, S. K., Boschung, J., Nauels, A., Xia, Y., Bex, V., and Midgley, P. M., pp. 1137–1216, Cambridge University Press, Cambridge, New York, 2013.

Coles, S.: An Introduction to Statistical Modeling of Extreme Values, Springer-Verlag London Ltd, iSBN: 1-85233-459-2, 2001.

Firing, Y. L. and Merrifield, M. A.: Extreme sea level events at Hawaii: Influence of mesoscale eddies, Geophysical Research Letters, 31, l24306 doi:10.1029/2004GL021539, 2004.

Gent, P. R. and McWilliams, J. C.: Isopycnal mixing in ocean circulation models, Journal of Physical Oceanography, 20, 150–155, 1990.

Greatbatch, R. J.: A note on the representation of steric sea level in models that conserve volume rather than mass, Journal of Geophysical Research, 99, 12 767–12 771, 1994.

Kienert, H. and Rahmstorf, S.: On the relation between Meridional Overturning Circulation and sea-level gradients in the Atlantic, Earth System Dynamics, 3, 109–120, doi: 10.5194/esd-3-109-2012, 2012.

Landerer, F. W., Jungclaus, J. H., and Marotzke, J.: Regional Dynamic and Steric Sea Level Change in Response to the IPCC-A1B Scenario, Journal of Physical Oceanography, 37, 296–312, doi: 10.1175/JPO3013.1, 2007.

Large, W. G. and Yeager, S. G.: Diurnal to decadal global forcing for ocean and sea-ice models; the datasets and flux climatologies, NCAR Technical Note TN 460 STR, http://www.clivar.org/organization/wgomd/resources/core/core-i (last access: 8 October 2008), 2004.

Maltrud, M., Bryan, F., Hecht, M., Hunke, E., Ivanova, D., McClean, J., and Peacock, S.: Global Ocean Modeling in the Eddying Regime Using POP, CLIVAR Exchange, 44, 5–8, 2008.

Pardaens, A. K., Gregory, J. M., and Lowe, J. A.: A model study of factors influencing projected changes in regional sea level over the twenty-first century, Climate Dynamics, 36, 2015–2033, doi: 10.1007/s00382-009-0738-x, 2011.

355 Rhein, M., Rintoul, S., Aoki, S., Campos, E., Chambers, D., Feely, R. A., Gulev, S., Johnson, G. C., Josey, S., Kostianoy, A., Mauritzen, C., Roemmich, D., Talley, L. D., and Wang, F.: Observations: Ocean, in: The Scientific Basis, Contribution of Working Group I to the Fifth Assessment Report of the Intergovernmental Panel on Climate Change, edited by Stocker, T. F., Qin, D., Plattner, G.-K., Tignor, M., Allen, S. K.,

360 Boschung, J., Nauels, A., Xia, Y., Bex, V., and Midgley, P. M., pp. 255–316, Cambridge University Press, Cambridge, New York, 2013.

Slangen, A., Katsman, C. A., van de Wal, R. S. W., Vermeersen, L. L. A., and Riva, R. E. M.: Towards regional projections of twenty-first century sea-level change based on IPCC SRES scenarios, Climate Dynamics, 38, 1191–1209, doi:10.1007/s00382-011-1057-6, 2012.

365 Slangen, A., Carson, M., Katsman, C. A., van de Wal, R. S. W., Koehl, A., Vermeersen, L. L. A., and Stammer, D.: Projecting twenty-first century regional sea-level changes, Climate Change, 124, 317–332, doi:10.1007/s10584-014-1080-9, 2014.

Smith, R. S. and Gregory, J. M.: A study of the sensitivity of ocean overturning circulation and climate to freshwater input in different regions of the North Atlantic, Geophysical Research Letters, 26, l15701

370 doi:10.1029/2009GL038607, 2009.

Sterl, A., Severijns, C., van Oldenborgh, G. J., Dijkstra, H., Hazeleger, W., van den Broeke, M., Burgers, G., van den Hurk, B., van Leeuwen, P., and van Velthoven, P.: When can we expect extremely high surface temperatures?, Geophysical Research Letters, 35, l14703 doi: 10.1029/2008GL034071, 2008.

Suzuki, T., Hasumi, H., Sakamoto, T. T., Nishimura, T., Abe-Ouchi, A., Segawa, T., Okada, N., Oka, A.,

375 and Emori, S.: Projection of future sea level and its variability in a high-resolution climate model: Ocean processes and Greenland and Antarctic ice-melt contributions, Geophysical Research Letters, 32, l19706 doi:10.1029/2005GL023677, 2005.

Van Oldenborgh, G. J., Te Raa, L., Dijkstra, H. A., and Philip, S. Y.: Frequency-or amplitude-dependent effects of the Atlantic meridional overturning on the tropical Pacific Ocean, Ocean Science, 5, 293–301,

380 doi:10.5194/os-5-293-2009, 2009.

Watson, C. S., White, N. J., Church, J. A., King, M. A., and Burgette, R. J.: Unabated global mean sea-level rise over the satellite altimeter era, Nature Climate Change, 5, 565–569, doi: 10.1038/NCLIMATE2635, 2015.

Weaver, A. J., Sedlacek, J., Eby, M., Alexander, K., Crespin, E., Fichefet, T., Philippon-Berthier, G., Joos, F., Kawamiya, M., Matsumoto, K., andK. Tachiiri, M. S., Tokos, K., Yoshimori, M., and Zickfeld, K.: Stability

385 of the Atlantic meridional overturning circulation: A model intercomparison, Geophysical Research Letters, 39, l20709 doi: 10.1029/2012GL053763, 2013.

Weijer, W., Maltrud, M. E., Hecht, M. W., Dijkstra, H. A., and Kliphuis, M. A.: Response of the Atlantic Ocean circulation to Greenland Ice Sheet melting in a strongly-eddying ocean model, Geophysical Research Letters, 39, l09606, doi: 10.1029/2012GL051611, 2012.

390 Yin, J., Schlesinger, M. E., and Stouffer, R. J.: Model projections of rapid sea-level rise on the northeast coast of the United States, Nature Geoscience, 2, 262–266, doi: 10.1038/ngeo462, 2009.

Yin, J., Griffies, S. M., and Stouffer, R. J.: Spatial Variability of Sea Level Rise in Twenty-First Century Projections, Journal of Climate, 23, 4585–4607, doi: 10.1175/2010JCLI3533.1, 2010.
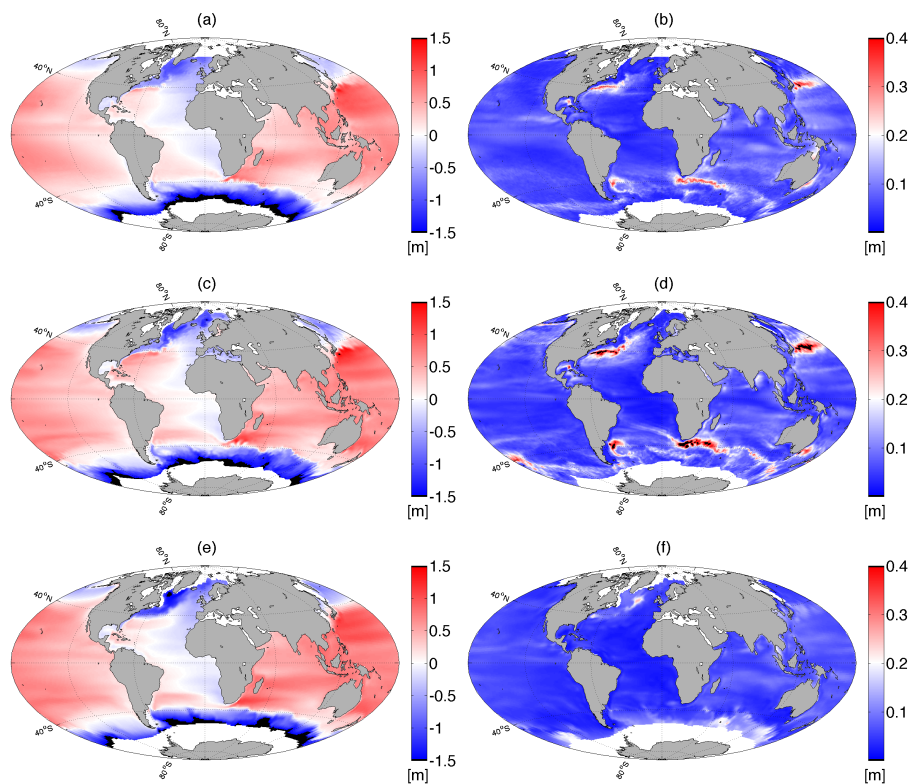
Figure 1. Mean sea surface height (SSH in meter) (a-c) and its standard deviation (b-d) over the years 1993-2012. (a,b) are derived from altimetry and (c-d) of the high-resolution simulation R_{021}. Panels (e,f) show the mean SSH and the standard deviation for the low-resolution simulation R_{021}^{low}, respectively.
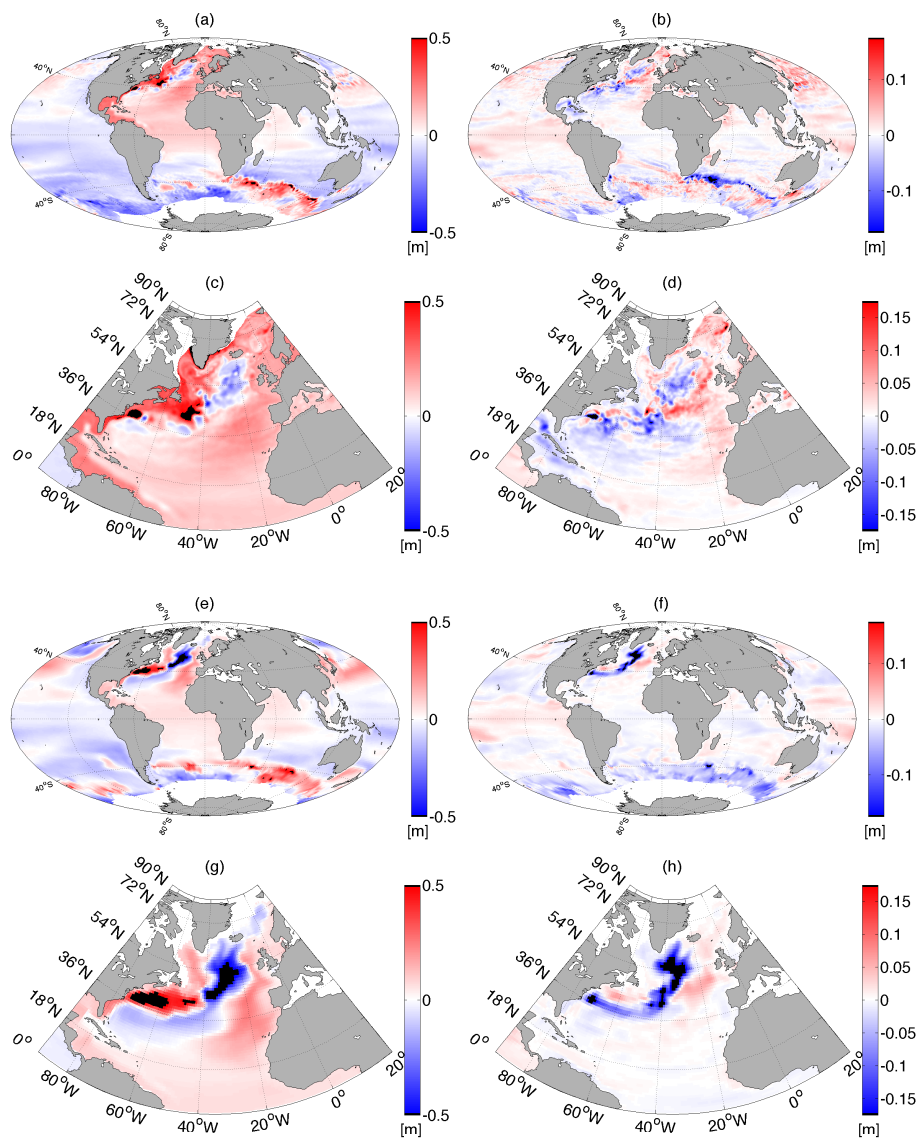
Figure 2. Change in the (a) mean and (b) standard deviation of modeled DSL in [m] between the periods 2081-2100 and 2001-2020 for the R_{021} simulation. The panels (c) and (d) are magnifications of (a) and (b) for the North Atlantic region. (e-h) Same as (a-d), but for the R_{021}^{low} simulation.
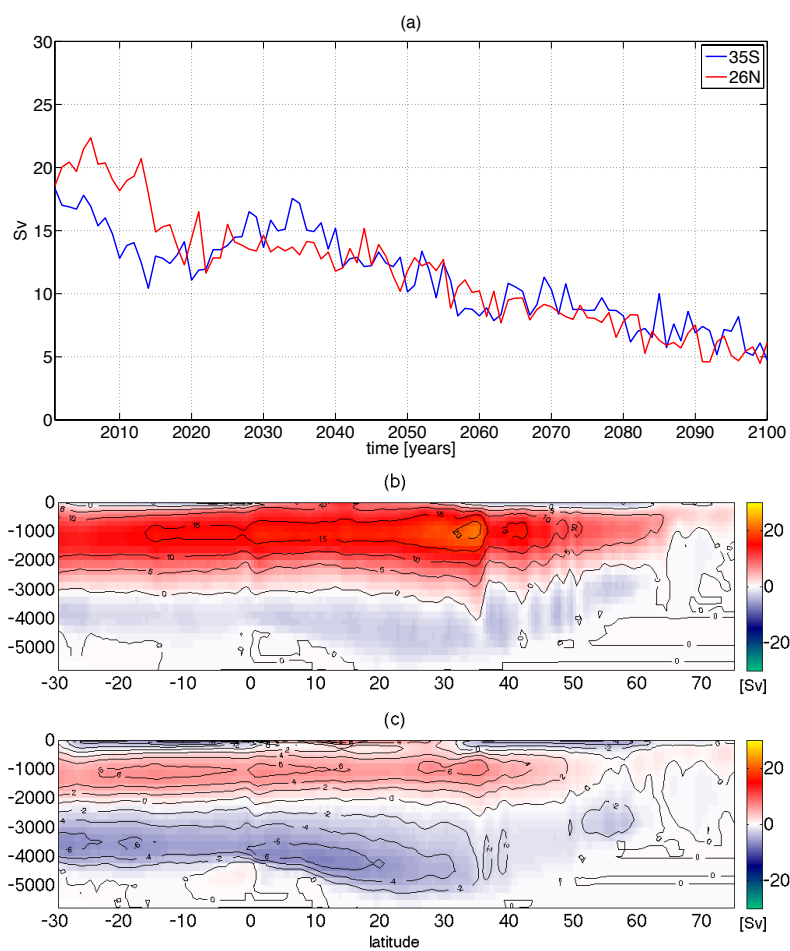
Figure 3. (a) Maximum AMOC strength at 35°S (blue) and 26°N (red) over the period 2000-2100. (b) Atlantic meridional overturning streamfunction (mean of years 2001-2020) (c) Same as (b) but over the period 2081-2100.
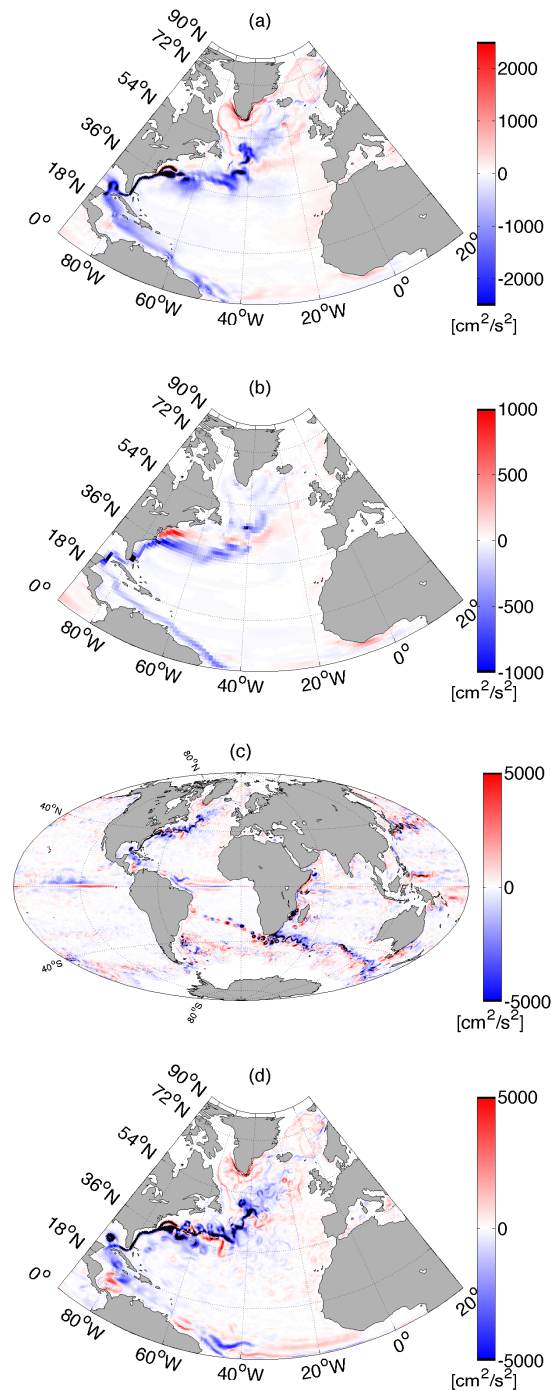
Figure 4. Difference of horizontal surface kinetic energy (energy flux per unit area) in cm^2/s^2 of the simulations (a) R_{021} and (b) R_{021}^{low} in the North Atlantic (mean of years 2081-2100 minus mean of years 2001-2020). (c) shows the difference in eddy kinetic energy (EKE) of the years 2090 and 2010 of R_{021}. Before computing EKE, the mean KE of the years 2080-2100 and 2000-2020 has been subtracted, respectively. (d) is the same as (c) showing only the North Atlantic.
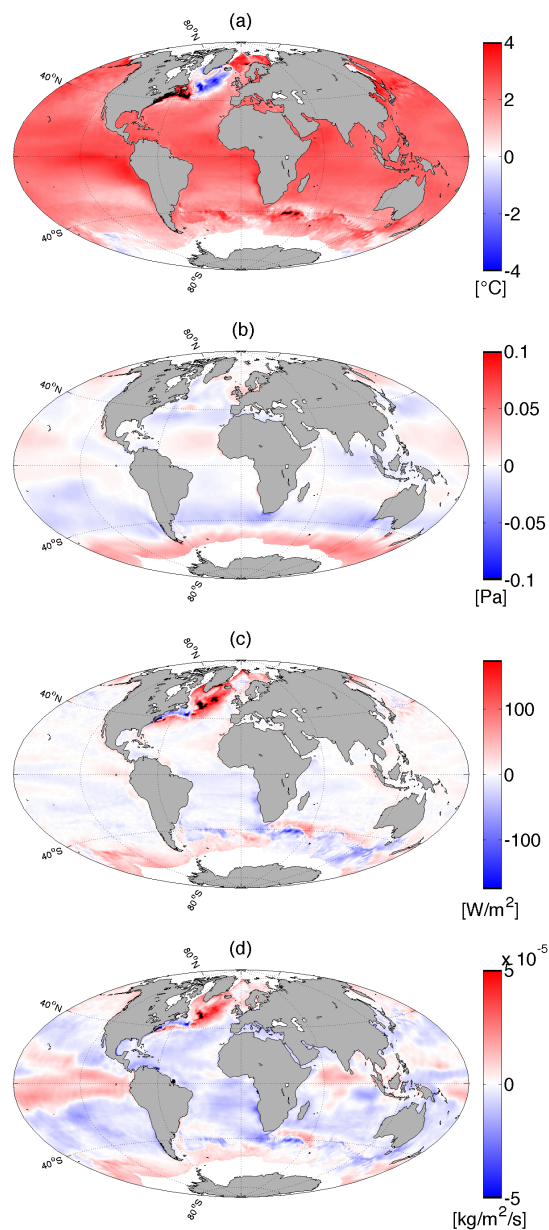
Figure 5. Change in (a) sea surface temperature ($^\circ C$), (b) zonal wind stress (Pa), (c) surface heat flux (W/m^2), and (d) surface freshwater flux ($kg/m^2/s$) for the R_{021} simulation; again the mean over the last 20 years (2081-2100) minus that over the first 20 years (2001-2020) is shown.
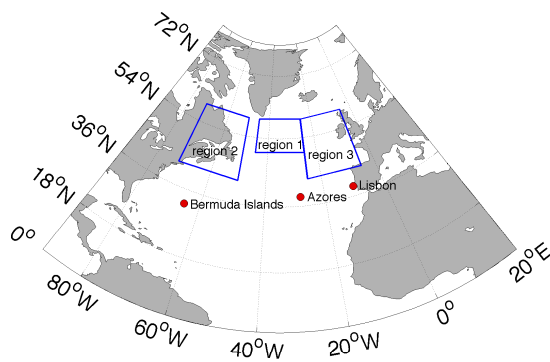
Figure 6. Regions and locations used for determining the PDFs and for the extreme value analysis.
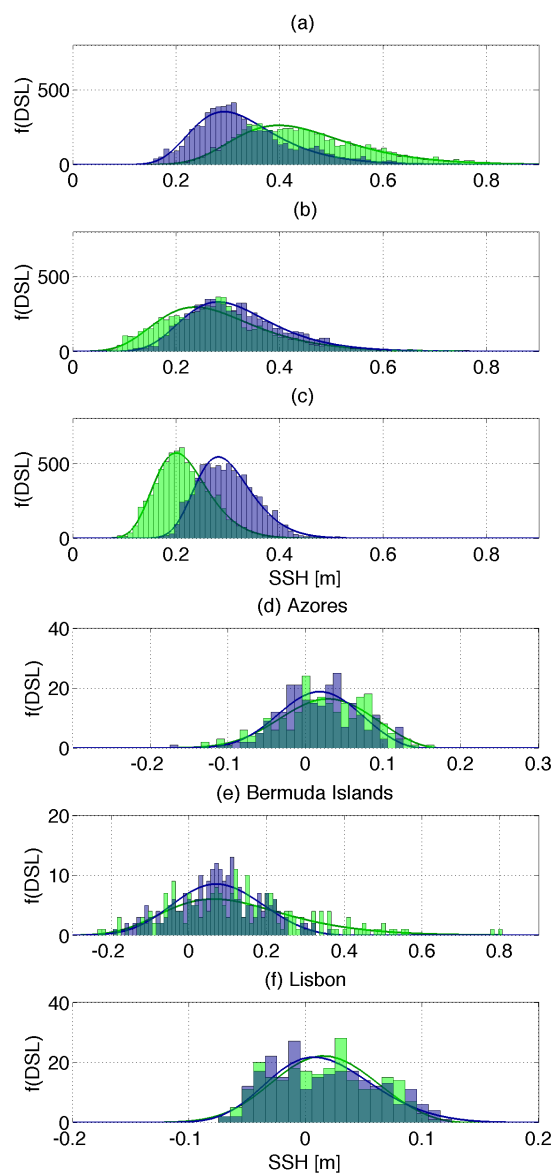
Figure 7. (a-c) Estimated Probability Density Function (PDF) of daily regional maximum DSL of simulation R_{021} in the three different regions in Fig. 6. In each plot, a maximum daily value over the region is identified after all variability with frequencies lower than 550 days has been filtered out. (d-f) Same, but for the locations indicated in Fig. 6 and using monthly maximum local DSL values derived from daily mean time series. The green histogram is the PDF for the first 20 years (2001-2020) and the blue histogram that for the last 20 years (2081-2100).
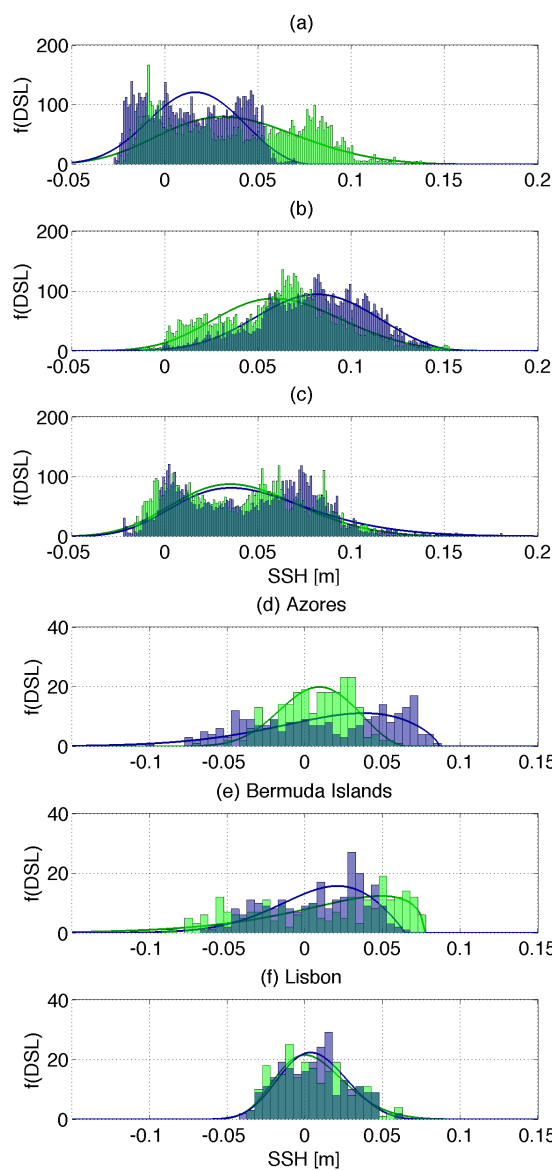
Figure 8. (a-c) Estimated Probability Density Function (PDF) of daily regional maximum DSL of simulation R_{021}^{low} in the three different regions in Fig. 6. In each plot, a maximum daily value over the region is used after all variability with frequencies lower than 550 days has been filtered out. (d-f) Same, but for the locations indicated in Fig. 6 and using monthly maximum local DSL values derived from daily mean time series. The green histogram is the PDF for the first 20 years (2001-2020) and the blue histogram that for the last 20 years (2081-2100).
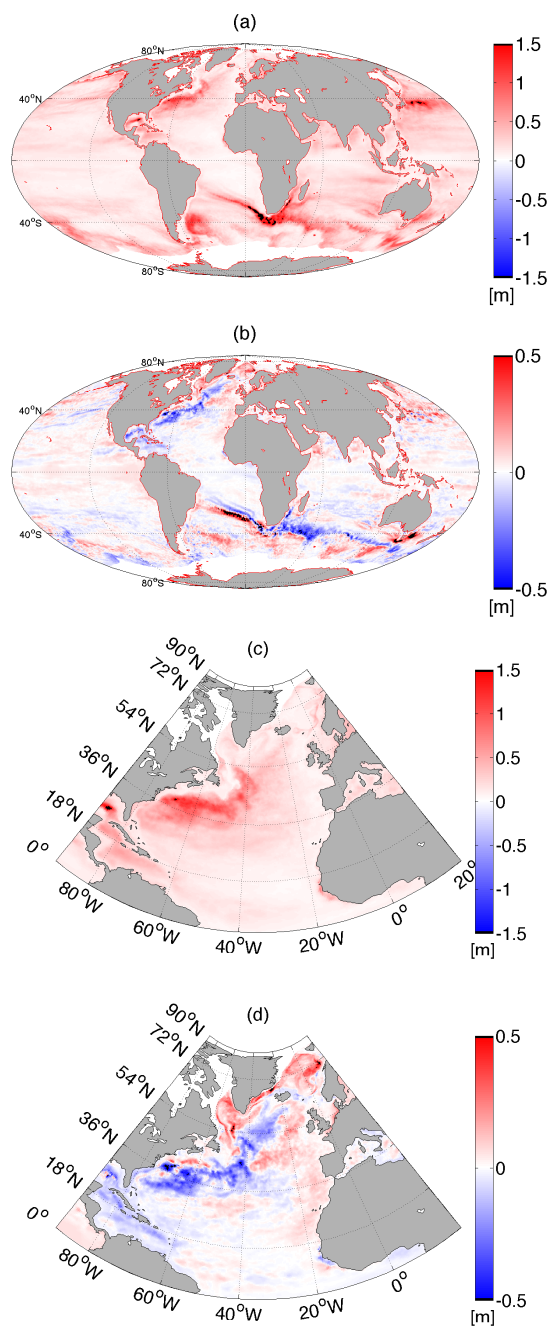
Figure 9. Extreme DSL values in [m] for a 10 year return time of simulation R_{021} for (a) the first 20 years
(2001-2020) and (b) the differences between the period 2081-2100 and 2001-2020. All signals with frequencies
lower than 550 days have been filtered out. The panels (c) and (d) are magnifications of (a) and (b) for the North
Atlantic region.
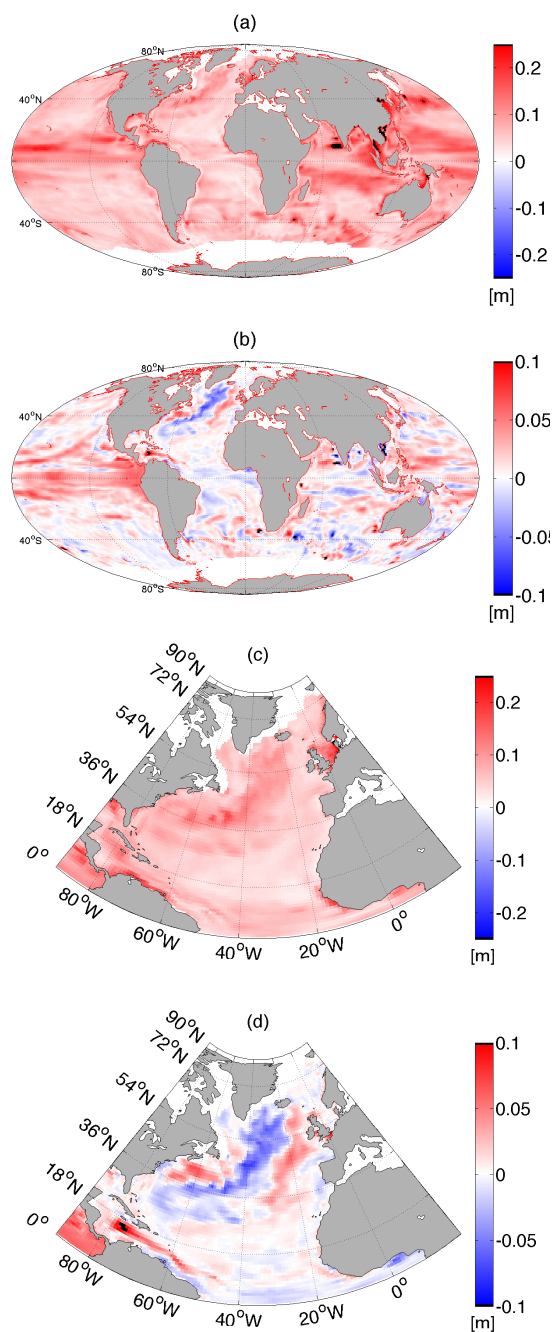
Figure 10. Extreme DSL values in [m] for a 10 year return time of simulation R_{021}^{low} for (a) the first 20 years (2001-2020) and (b) the differences between the period 2081-2100 and 2001-2020. All signals with frequencies lower than 550 days have been filtered out. The panels (c) and (d) are magnifications of (a) and (b) for the North Atlantic region.